Experimental investigation of dissociation pathways of cooled HeH^+ following valence electron excitation at 32 nm by intense free-electron-laser radiation

H. B. Pedersen,[1,*] L. Lammich,[1] C. Domesle,[2] B. Jordon-Thaden,[2] O. Heber,[3] J. Ullrich,[2] R. Treusch,[4] N. Guerassimova,[4] and A. Wolf[2]

[1]*Department of Physics and Astronomy, Aarhus University, DK-8000 Aarhus C, Denmark*

[2]*Max-Planck-Institut für Kernphysik, D-69117 Heidelberg, Germany*

[3]*Department of Particle Physics, Weizmann Institute of Science, 76100 Rehovot, Israel*

[4]*Hamburger Synchrotronstrahlungslabor at Deutsches Elektronen-Synchrotron, D-22607 Hamburg, Germany*

(Received 2 July 2010; published 16 August 2010)

The dissociation pathways of HeH^+ have been investigated below the first ionization continuum by photoabsorption at 32 nm, using fragment momentum imaging in a crossed-beams experiment at the free-electron laser in Hamburg (FLASH). Investigations were done both for ions with several vibrational levels excited in the ion source and for ions vibrationally cooled in an electrostatic ion trap prior to the irradiation. The product channels $He^+(1s) + H(nl)$ and $He(1snl) + H^+$ were separated and the $He(1snl) + H^+$ channel was particularly studied by coincidence detection of the He and H^+ fragments on two separate fragment detectors. At 32 nm excitation, the branching ratio between the product channels was found to be $\sigma_{He^+ + H}/\sigma_{He + H^+} = 0.96 \pm 0.11$ for vibrationally hot and 1.70 ± 0.48 for vibrationally cold ions. The spectra of kinetic energy releases for both channels revealed that photodissociation at 32 nm leads to high Rydberg states ($n \gtrsim 3$–4) of the emerging atomic fragments irrespective of the initial vibrational excitation of HeH^+. The fragment angular distributions showed that dissociation into the $He + H^+$ channel mostly (~70%) proceeds through $^1\Pi$ states, while for the $He^+ + H$ channel $^1\Sigma$ and $^1\Pi$ states are of about equal importance.

DOI: 10.1103/PhysRevA.82.023415 PACS number(s): 33.80.Gj

I. INTRODUCTION

Photoabsorption by molecular cations in the xuv and soft x-ray region initiates dissociation through manifolds of coupled excited states that arise from the excitation of the molecular valence electrons. The pathways of the dissociating system through these excited states can be strongly influenced by nonadiabatic couplings between electronic and nuclear motions [1]. Thus, in this region, the dissociation dynamics goes beyond the Born-Oppenheimer approximation where a separate description of the electronic and nuclear degrees of freedom is assumed. Simple molecular cations are model systems to study such interactions, since detailed aspects of their nonadiabatic couplings can be theoretically isolated [2,3] and compared to experimental observations.

In this paper, we report a kinematically complete investigation of the photodissociation of the simplest heteronuclear molecular ion HeH^+ at 32 nm (38.7 eV), addressing explicitly the dissociation dynamics through the manifold of singly excited states below the first ionization continuum, $He^+(1s) + H^+$, in a process schematically written as

$$\begin{aligned} HeH^+(^1\Sigma) + 32\,\text{nm} &\rightarrow [HeH^+(^1\Sigma/^1\Pi)]^* \\ &\rightarrow \begin{cases} He(1snl) + H^+, \\ He^+(1s) + H(nl). \end{cases} \end{aligned} \quad (1)$$

Figure 1 illustrates the photoabsorption and dissociation process through this excited state manifold. In a simplified view, the photoabsorption instantaneously brings an electron from the 1σ orbital of $HeH^+(1\sigma^2\,^1\Sigma)$ into an excited orbital of σ or π symmetry. Ionization or double excitation of the 1σ electrons only happens at photon energies beyond ~40 eV [4]. During the subsequent dissociation process, energy is distributed between kinetic energy and internal energy of the fragments in a process where nonadiabatic interactions can play a significant role.

HeH^+ is astrophysically significant and it appears, for instance, as a molecular coolant in models of the early universe [5], and it is assumed to exist in astrophysical plasmas near strong xuv sources like planetary nebulae [6]. Moreover, the excited states of HeH^+ involved in the photodissociation process are of relevance for evaluating the molecular contributions to the electron energy spectrum of β-decaying T_2 [7,8] to be used in upcoming measurements of the mass of the electron neutrino [9]. Finally, HeH^+ is isoelectronic with the simplest neutral molecule H_2 (D_2) presently under intense study with respect to molecular dynamics in strong laser fields. Thus, while dissociation dynamics after strong-field ionization into $H_2{}^+$ is being studied in great detail [10,11], the possible strong-field excitation into the associated $H(nl) + H(n'l')$ state manifold is unexplored in these experiments since only charged fragments are detectable. This dissociation dynamics, however, is mimicked (albeit without the additional dressing of the states by an intense laser field) by the dissociation of HeH^+ through the excited-state manifold reached by xuv photoabsorption as depicted in Fig. 1. Experimentally, we observe the momenta of atomic fragments (He, H, and H^+) from isolated photoabsorption processes in a dilute fast-moving beam of HeH^+ ions crossed by short pulses of xuv radiation from the free-electron laser in Hamburg (FLASH) [12,13]. The feasibility of the experiment relies largely on the extreme intensity of the xuv pulses from this free-electron laser source.

*Corresponding author: hbjp@phys.au.dk

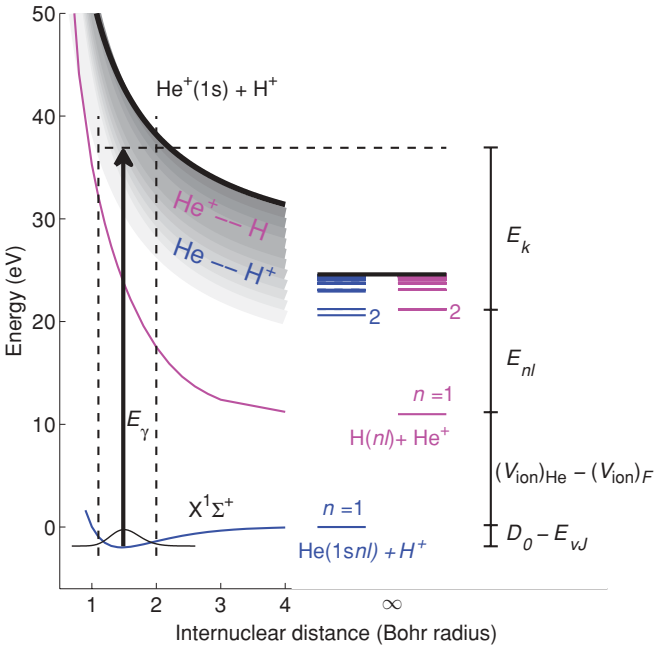

FIG. 1. (Color online) Photoabsorption and dissociation of HeH^+ by 32 nm (38.7 eV) irradiation. The photoabsorption process is indicated by the vertical arrow and the approximate Franck-Condon region of internuclear distance for the vibrational ground state ($v = 0$) is marked by the vertical dashed lines. The dissociation process proceeds through a manifold of coupled excited states indicated by the shaded area (see Refs. [2,3] for actual states), finally converting the available energy after the photoabsorption ($E_\gamma - D_0 + E_{vJ}$) into kinetic energy, E_k, and internal energy, $E_{nl} + (V_{\rm ion})_{\rm He} - (V_{\rm ion})_F$ (F = H, He; $V_{\rm ion}$ is the ionization potential), of the fragments [see also Eq. (9)].

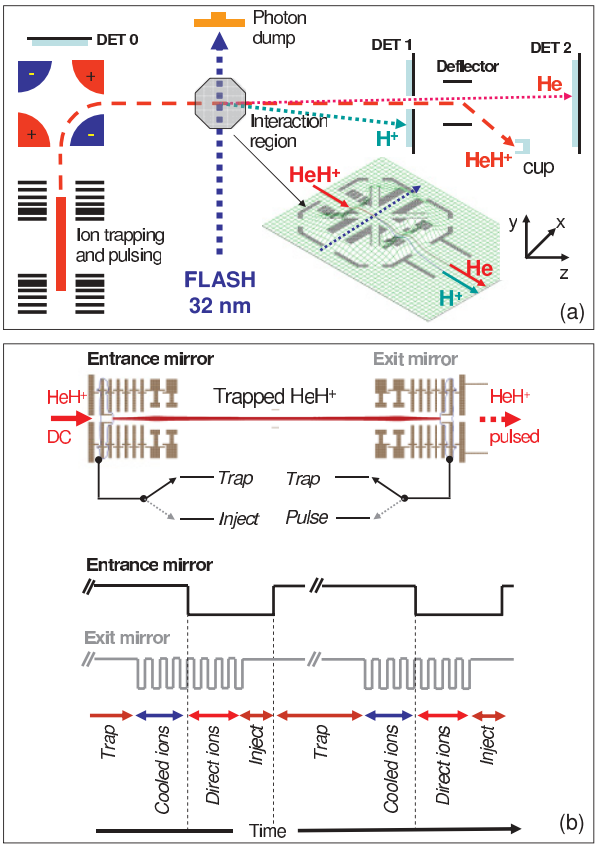

FIG. 2. (Color online) Experimental setup and timing scheme for the crossed-beams setup at FLASH. (a) Schematic illustration of a part of the TIFF setup [15] including the electrostatic ion trap, interaction region, and fragment detectors. (b) Operation of the ion-trap mirrors to generate trains of cooled and direct ions synchronized with the FLASH time structure.

Experiments were performed both for ions in the vibrational ground state (cooled), for which the Franck-Condon region is indicated in Fig. 1, and for vibrationally hotter ions, thereby probing different regions of initial internuclear distances in the dissociating molecular ion.

The present type of experiment obtains information related to both the photoabsorption and the dynamics of the subsequent dissociation process. The photoabsorption is characterized through an estimate of the absolute cross section, as was performed in an earlier measurement [14], and through analysis of the nature of the major absorbing states ($^1\Sigma$ or $^1\Pi$) as revealed by the momenta of emerging fragments. The dynamics of the dissociation process is addressed by the measurement of the nature of the final states, that is, the dissociation channel ($He^+ + H$ or $He + H^+$) and the fragment excitations [He($1snl$) and H(nl)]; both aspects hold information about the nonadiabatic interactions influencing the dissociation pathways.

II. EXPERIMENT

A. Setup

The experiment was conducted at the trapped ion fragmentation with an FEL (TIFF) setup [15] installed at the plane grating monochromator beamline PG2 [16] of the FLASH [12,13] at the Deutsches Elektronen Synchrotron (DESY) in Hamburg. The ions were generated on a high voltage potential by a newly added duoplasmatron-type ion source [17] operated with a gas inlet of H_2 (15%) and He (85%), at an estimated total pressure of 0.1 mbar, and with an electric discharge sustained at 90 V/100 mA. From the plasma, ions were extracted, accelerated to ground potential, and mass analyzed in a magnetic field to form a collimated beam of HeH^+ at $E_0 = 4.2$ keV kinetic energy and with a typical current of 100–150 nA.

Figure 2(a) shows schematically the experimental setup around the ion-photon interaction region. The mass-selected beam of HeH^+ was guided into a linear electrostatic ion trap [15,18] composed of two opposing focusing electrostatic mirrors. As shown in detail in Fig. 2(b), the ion-trap setup is used both to store ensembles of ions (operation of the entrance mirror) for a sufficient time to allow for radiative cooling of rovibrational motion initially excited upon production in the ion source, and to generate short ion pulses (operation of the exit mirror) synchronized to the FLASH time structure. During injection, the first electrode of the entrance mirror is switched to a low potential (3.7 kV) that allows the dc ion beam to enter the trap. The part of the ion beam located between the electrostatic mirrors is trapped by switching this electrode to a higher potential (4.6 kV). Efficient and stable trapping was

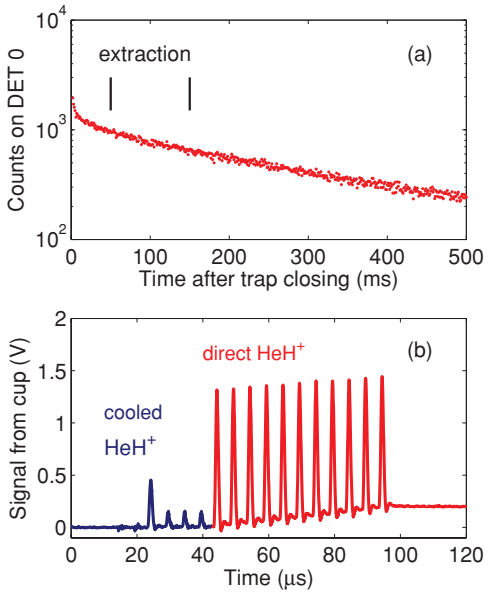

FIG. 3. (Color online) Ion trapping and pulsing. (a) Neutrals detected with DET 0 as a function of time after closing the ion trap. The spectrum was integrated over 300 injections and was obtained with a pressure of $\sim 2 \times 10^{-9}$ mbar. At long times a single exponential decay is observed with a characteristic $(1/e)$ decay time of about 400 ms. The vertical lines indicate the times of extraction used in the present experiment (50 and 150 ms). (b) Signal from the ion cup [marked in Fig. 2(a)] after charge amplification and pulse shaping (differentiation) following extraction at 50 ms.

ensured by monitoring the stored ions on a short time scale by an electrostatic pickup positioned in the trap center and on a long time scale by observing the decay of the trapped ion beam using Detector (DET) 0 [Fig. 2(a)] to register neutral fragments created in collisions between the trapped ions and residual gas molecules; the measured time dependence is shown in Fig. 3(a).

After a trapping period of 50–150 ms, a train of pulses of cooled HeH^+ ions was extracted by rapidly switching the outermost electrode in the exit mirror between two high voltage levels (4.6 and 2.8 kV). After a cooling time of $\geqslant$50 ms in the electrostatic ion trap, thermal equilibrium at $\sim$300 K can be assumed for the vibrational motion, and essentially all HeH^+ ions can be considered to be in the vibrational ground state $v = 0$: the radiative lifetimes of vibrational levels v of the electronic $X^1\Sigma$ ground state of HeH^+ can be estimated [19,20] to $\sim$9 ms for $v = 1$, $\sim$6 ms for $v = 2$, and smaller for the higher vibrational levels. When all cooled ions had been extracted from the ion trap, here after four extractions of 1-μs pulses, the entrance mirror was reopened and additional pulses were transferred directly from the ion source to the interaction region. After the ion-photon crossing, the ion pulses were bent into a Faraday cup; Fig. 3(b) shows the signal of the cooled and directly transferred ion pulses as observed with this cup after charge integration and electronic signal differentiation. The linear density of the directly transferred pulses ($8–12 \times 10^3$ cm^{-1}) is equivalent to a dc current of 50–75 nA at the interaction region.

From the FLASH, trains of 30 short ($\sim$10–50 fs) pulses of 7–15 μJ at 32 ± 0.5 nm (38.7 ± 0.6 eV), separated by 5 μs, were delivered at a 5-Hz repetition rate and with linear polarization along the ion-beam direction. The photons were guided through the PG2 beamline with the monochromator operated in zero order with an estimated transmission of $T = 0.4 \pm 0.1$ of the original photon intensity, yielding 0.5–1×10^{12} photons per pulse in the beam-crossing region. In the present experiment, 24 photon pulses were used in each train: 4 pulses were crossed by cooled ions, 18 were crossed by directly transferred (vibrationally excited) ions and 2 were used for background measurements. The photon pulses were dumped in a negatively biased Cu structure, a signal from which was used to monitor the photon pulses after the monochromator [15]. To ensure spatial overlap of the two beams, their vertical intensity profiles were measured by a movable 1-mm-wide slit positioned at 45° degrees to both beam directions [15]. The beams were well characterized by nearly cocentric Gaussian distributions of widths (rms) $\sim$0.75 mm.

Photofragments were detected on two time- and position-sensitive multihit detectors, labeled DET 1 and DET 2 in Fig. 2(a), which were located at $L_1 = 0.263$ m and $L_2 = 0.872$ m from the interaction region; for more details on these detectors see Ref. [15]. Due to the mass difference of hydrogen and helium, the dissociation kinematics is such that the H^+-H fragments and He-He^+ fragments are naturally separated by hitting on the two different detectors DET 1 and DET 2, respectively. Thus, the observed momentum releases (Sec. II B) on DET 1 were only compatible with the fragments being H^+-H. The He^+ ions were deflected together with the main HeH^+ beam such that only He fragments were detected on DET 2.

The crossing region of the photon and ion beams was biased to a controlled local electrical potential V_c, and the kinetic energy of the reacting ions was $E_I = E_0 - eV_c$. Moreover, when $V_c > 0$, an electrical barrier was applied downstream of the the ion-beam direction to prevent ions generated by photoionization of the residual gas to reach the fragment detectors [15]; some details of the interaction region and the applied electrical barrier can be seen in Fig. 2(a).

B. Fragment momentum imaging

For a particle impacting on DET i $(i = 1, 2)$, we register both the time of flight t_i relative to the moment of interaction as well as the transverse position of impact (x_i, y_i) on the detector surface. To analyze the kinematics of the fragments, we introduce a set of normalized coordinates (ρ_i, τ_i) [15] relative to an undeflected and unretarded fragment moving with beam velocity v_I; explicitly, $\rho_i = r_i/L_i$ and $\tau_i = t_i/(L_i/v_I)$.

In the particular cases where either the bias $V_c = 0$ or the fragment charge $q_F = 0$, the momentum releases from the photofragmentation process in the directions parallel and transverse to the laser polarization (along the ion-beam direction) are obtained from the relations

$$\begin{aligned} \Delta p_F^{\parallel}/p_F &= (\Delta p_F/p_F)\cos\theta_F = 1/\tau_i - 1, \\ \Delta p_F^{\perp}/p_F &= (\Delta p_F/p_F)\sin\theta_F = \rho_i/\tau_i, \end{aligned} \tag{2}$$

where $p_F = m_F v_I$ is the momentum of the undisturbed fragment. Figures 4(a) and 4(b) display momentum images as observed on DET 1 (H and H^+ fragments) for (a) directly

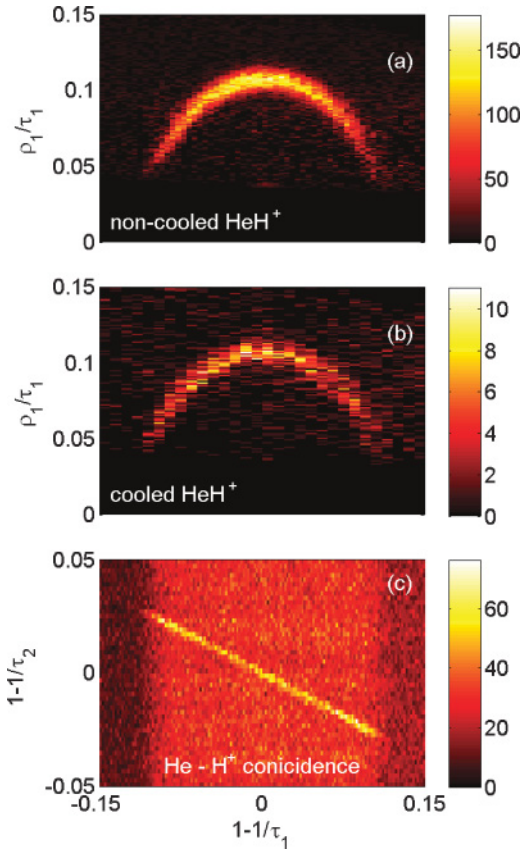

FIG. 4. (Color online) Momentum imaging and coincidence detection at $V_c = 0$. (a) Momentum image of dissociating HeH^+ after direct transfer from the ion source (vibrationally hot) and (b) after 50–150 ms cooling in the electrostatic ion trap. (c) Identification of true coincidences on a straight line [Eq. (6)] in the correlation of longitudinal momentum releases observed on DET 1 and DET 2.

transferred and (b) cooled HeH^+ obtained with $V_c = 0$. The cutoff in the transverse momentum at low values results from the geometric acceptance of DET 1 with the central hole [15]. Evidently, the total momentum release and fragmentation angle relative to the laser polarization can be obtained through

$$\left(\frac{\Delta p_F}{p_F}\right)^2 = \left(\frac{\rho_i}{\tau_i}\right)^2 + \left(\frac{1}{\tau_i} - 1\right)^2, \tag{3}$$

$$\tan\theta_F = (\rho_i/\tau_i)/(1/\tau_i - 1), \tag{4}$$

The kinetic energy of the fragment is given by $E_F = \Delta p_F^2/2m_F$, while the total kinetic energy release in the two-body dissociation process is obtained as

$$E_k = \frac{\Delta p_F^2}{2\mu}, \tag{5}$$

where $\mu = m_H m_{He}/(m_H + m_{He})$ is the reduced mass. By requiring coincidence between impacts on DET 1 and DET 2, a fraction of events belonging to the to the dissociation channel $He(1snl) + H^+$ (coincidence of H^+ on DET 1 and He on DET 2) could be isolated from the $He^+ + H(nl)$ channel, which cannot produce such coincidences because He^+ ions are prevented from reaching DET 2. Moreover, the background from neutralizations in the residual gas was reduced significantly by this coincidence requirement. In Fig. 4(c), the identification of coincidence events is illustrated by a diagram showing the parallel momentum release $1 - 1/\tau_i$ recorded with each of the two detectors. Due to momentum conservation, the coincident events localize on a straight line given by

$$1 - 1/\tau_2 = -\frac{m_H}{m_{He}}(1 - 1/\tau_1). \tag{6}$$

A narrow cut around this line isolates the true coincidences belonging to the same dissociation event, as opposed to false coincidences that appear as a bright band in Fig. 4(c). Similar cuts derived from momentum conservation in the two transverse directions were also implied in the final identification of true coincidences.

The coincidence detection allows a higher resolution in the evaluation of the energy release [Eq. (5)] and dissociation angle [Eq. (4)] since the laboratory coordinates of the dissociation points (x_0, y_0, z_0) can be directly evaluated for each ion, thereby eliminating broadening due to the finite sizes of the ion and photon beams. Explicitly, defining a parametric time (t_s) through $1/t_s = m_H/t_1 + m_{He}/t_2$, the laboratory coordinates of the dissociation event were calculated as

$$\begin{aligned} x_0 &= [(x_1/t_1)m_H + (x_2/t_2)m_{He}]\,t_s, \\ y_0 &= [(y_1/t_1)m_H + (y_2/t_2)m_{He}]\,t_s, \\ z_0 &= [(L_1/t_1)m_H + (L_2/t_2)m_{He} - v_I m_I]\,t_s, \end{aligned} \tag{7}$$

which were then used in the evaluation of τ_i and ρ_i for the events identified as true coincidences.

III. RESULTS

A. Branching of dissociation channels

To identify the fragments on DET 1 ($H\text{-}H^+$) and thus the dissociation channel [Eq. (1)], measurements with a local potential applied to the interaction region were performed. Due to the local potential, a fragment of mass m_F and charge q_F will emerge after the interaction region with a momentum in the direction parallel to the ion-beam direction of

$$p_F^{\parallel}/p_F = \sqrt{(1 + \Delta p_F^{\parallel}/p_F)^2 + \eta_F}, \tag{8}$$

where $\eta_F = (q_F/m_F)(m_I V_c/E_I)$, which consequently imposes a shift in the time of flight of the fragment to the detector depending on the fragment mass-to-charge ratio. Figures 5(a) and 5(b) show the momentum images observed with DET 1 with a local potential of $V_c = 300$ V applied to the interaction region for both vibrationally hot and cooled ions. For H^+, $\eta_{H^+} = 0.382$, which effectively leads to a shift of the observed distribution of $1 - 1/\tau_1$ to be centered at [15] $1 - \sqrt{1 + \eta_{H^+}} = -0.176$, while the distribution of H fragments remains centered around $1 - 1/\tau_1 = 0$. The actual shift of the distribution of H^+ fragments will be smaller than -0.176 both because of the finite extent of the zone with the local potential and because of the barrier after the interaction region. In Figs. 5(a) and 5(b), the distribution forming a semicircle around $1 - 1/\tau_1 = 0$ can thus be identified as H fragments originating from the breakup into $He^+ + H(nl)$. Accordingly,

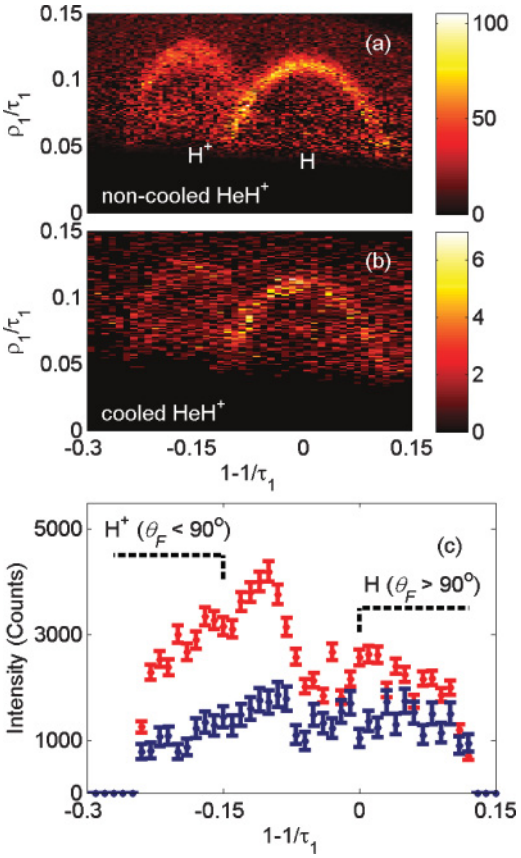

FIG. 5. (Color online) Branching of dissociation channels analyzed by momentum imaging with a local potential of $V_c = 300$ V at the interaction region. Momentum images shown for (a) vibrationally hot and (b) vibrationally cooled HeH^+ after photodissociation at 32 nm, and (c) the projected distributions on the axis of the longitudinal momentum release for vibrationally hot [upper (red) points] and vibrationally cold [lower (blue)points] ions; the spectrum for cold ions was multiplied by a factor of 15. The marked regions in (c) are completely dominated by H^+ or H fragments, respectively.

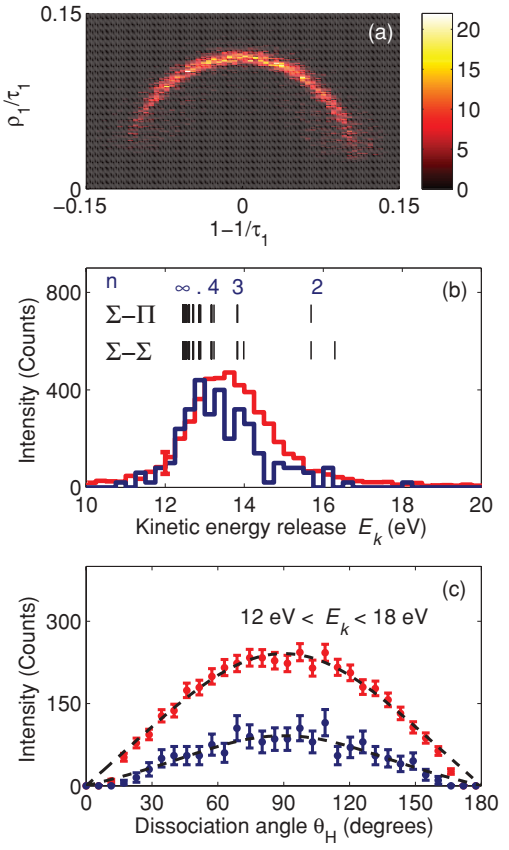

FIG. 6. (Color online) Analysis of the photodissociation of HeH^+ at 32 nm into $He(1snl) + H^+$ from coincidence impacts of H^+ on DET 1 and He on DET 2 obtained with $V_c = 0$. (a) Momentum image observed on DET 1 with a coincidence required on DET 2. (b) Fragment kinetic energy release for vibrationally hot (red line) and cold (blue line) ions. For comparison, the distribution for cold ions has been multiplied by a factor of 20. The vertical lines indicate the expected E_k for various fragment excitation energies E_{nl} and $E_{vJ} = 0$. (c) Angular distribution of fragments relative to the laser polarization direction for hot (red) and cold (blue) HeH^+ ions. The dotted lines show fits with Eq. (11) to the experimental distributions.

the similar distribution centered at $1 - 1/\tau_1 \sim -0.15$ results from H^+ fragments from a breakup into $He(1snl) + H^+$. For the H^+ fragments, the electrical barrier applied after the interaction region along with a small derivation from the ideal ion-beam path through the center of the electrodes of the interaction region makes the momentum image more blurred than the distribution of H fragments.

The two distributions overlap in a region of measured longitudinal momentum release around $1 - 1/\tau_1 \sim -0.10$. However, more than half of the events of both H^+ and H are completely separated using the local potential. Figure 5(c) shows the projection of the momentum distributions on the axis of longitudinal momentum release, and the regions covering half of each fragment distribution are indicated: $1 - 1/\tau_1 \leqslant -0.15$ for H^+ and $1 - 1/\tau_1 \geqslant 0$ for H. Since the distributions of the fragments are naturally symmetric with respect to the direction of the laser polarization, we obtain the ratio of H^+ to H fragments from the intensity in these two regions. This ratio translates directly into the branching ratio for the two major dissociation channels of HeH^+. Thus, for vibrationally hot ions, we obtain $\sigma_{He^+ + H}/\sigma_{He+H^+} = 0.96 \pm 0.11$ while for vibrationally cooled ions the result is $\sigma_{He^+ + H}/\sigma_{He+H^+} = 1.70 \pm 0.48$.

B. $He(1snl) + H^+$

As explained in Sec. II B, events belonging to the dissociation channel $He(1snl) + H^+$ were isolated from both events related to dissociation into $He^+(1s) + H^+(nl)$ and from background events by requiring a coincidence between impacts on DET 1 and DET 2, imposing the criteria of momentum conservation [Eq. (6)] and applying the dissociation point correction [Eq. (7)]. Figure 6(a) displays the momentum image on DET 1 under these conditions. The resulting spectra of kinetic energy releases as obtained through Eq. (5) are shown in Fig. 6(b) for both hot and cold ions. By conservation of energy, this kinetic energy release is related to the photon

energy $E_\gamma = 38.7$ eV and the initial rovibrational excitation E_{vJ} of the HeH^+ by

$$E_k = E_\gamma - E_{nl} - [(V_{\rm ion})_{\rm He} - (V_{\rm ion})_F] - D_0 + E_{vJ}, \quad (9)$$

where $(V_{\rm ion})_{\rm He} = 24.59$ eV and $(V_{\rm ion})_F$ are the ionization potentials of He and the neutral fragment (F = He, H), and $D_0 = 1.85$ eV [6] is the dissociation energy of HeH^+ in the electronic ground state. For vibrationally hot ions, the distribution of kinetic energy peaks at ~13.5 eV, extends to ca. 12–12.5 eV toward lower energies, and reaches 15–16 eV toward higher energies. For vibrationally cooled ions, the spectrum is similar on the low-energy side; however, it peaks at ca. 12 eV and extends only to 14–15 eV. An overall broadening of the distributions of kinetic energy, as evident by the tails of the distributions reaching below the threshold (12.5 eV), is consistent with the spread in the photon energy (±0.6 eV) from FLASH.

Evidently, for both hot and cold HeH^+, dissociation in this channel is preferred into final He states of relatively high excitation. For the cooled ions, the distribution peaks toward $n \gtrsim 4$. For the hot ions, a definitive statement on the fragment excitation cannot be made due to the uncertainty of the vibrational excitation (E_{vJ}); however, a preference for high excitations (at least $n \gtrsim 3$) can be inferred. Assuming similar final-state distributions for the different vibrational states, the difference between the two spectra shows explicitly the effect of vibrational cooling. Thus, under this assumption, the cooling of the HeH^+ amounts to ca. 0.7 eV, corresponding to 3–4 quanta of vibrational excitation [21,22].

In Fig. 6(c) the distributions of the dissociation angle relative to the laser polarization are analyzed. Photoabsorption into a particular final state of either $^1\Sigma$ or $^1\Pi$ symmetry can be represented by a distribution of the form [23]

$$P(\theta_F, \beta) = \left(\frac{1}{2} - \frac{\beta}{4} + \frac{3\beta}{4}\cos^2\theta_F\right)\sin\theta_F, \quad (10)$$

characterized by the anisotropy parameter β. For a prompt dissociation, $\beta = 2$ is expected for $^1\Sigma$–$^1\Sigma$ transitions, and $\beta = -1$ for $^1\Sigma$–$^1\Pi$ transitions. To quantify the experimental observation, we model the observed spectra with a function of the form

$$P_m(\theta_F) = a_2 P(\theta_F, 2) + a_{-1} P(\theta_F, -1) \quad (11)$$

and obtain the coefficients (a_2, a_{-1}) through a least-squares fit. For the vibrationally cold (hot) ions, we find $a_2 = 24 \pm 6\%$ ($30 \pm 2\%$) and $a_{-1} = 76 \pm 6\%$ ($70 \pm 2\%$), where the results are consistent with our previous measurement with hot ions [14].

C. $He^+(1s) + H(nl)$

As shown in Figs. 5(a) and 5(b), the two photofragment channels of Eq. (1) were separated on DET 1 through measurements with a local potential ($V_c = 300$ V) at the interaction region. In these momentum images the H fragments from $He^+(1s) + H(nl)$ are localized on a semicircle centered at $1 - 1/\tau_1 = 0$.

A significant fraction of the momentum image can be assigned to H fragments alone (corresponding to $\theta_{\rm H} \geqslant 70^\circ$ and beyond), and the data from this region are used to further analyze the dynamics of this particular dissociation channel, albeit with lower resolutions in kinetic energy [Eq. (5)] and angle [Eq. (4)] due to the finite sizes of the ion and photon beams. Figure 7(a) displays the resulting spectra of kinetic energy release. The broadening of ca. ±1 eV due to the finite beam sizes in addition to the ±0.6 eV from the photon energy is clearly recognized toward lower energy. Similar to the results for the channel $He(1snl) + H^+$ (Fig. 6), both hot and cold ions show a clear preference for dissociation into final states of high excitation. The tendency of the cold ion spectrum to peak even more toward higher excitation energy (lower E_k) is also observed.

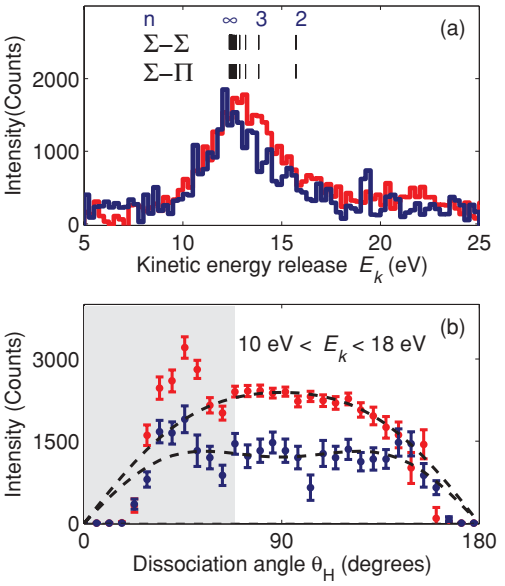

FIG. 7. (Color online) Analysis of the photodissociation of HeH^+ at 32 nm into the $He^+ + H(nl)$ from impacts of H fragments on DET 1 as obtained with a local potential of $V_c = 300$ V at the interaction region (see also Fig. 5). (a) Fragment kinetic energy release for vibrationally hot (red line) and vibrationally cold (blue line) ions. The distribution for cold ions has been multiplied by a factor of 40. (b) Angular distribution of fragments relative to the laser polarization direction for hot (red) and cold (blue) HeH^+ ions. The shaded area marks the region of overlap of the two dissociation channels (see also Fig. 5). The dashed lines show fits with Eq. (11) to the experimental distributions for $\theta_{\rm H} > 70^\circ$.

Figure 7(b) shows the angular distribution of H fragments relative to the laser polarization. The region where the two dissociation channels cannot be clearly separated [see also Figs. 5(a) and 5(b)] with a bias of $V_c = 300$ V, is shaded and excluded from the analysis. Interestingly, the angular distributions appear to be different from the corresponding results obtained for the $He + H^+$ channel [Fig. 6(c)], indicating a different importance of $^1\Sigma$ and $^1\Pi$ states in the absorption process leading to this channel. From a least-squares fit with the model of Eq. (11) to the experimental data, we obtain coefficients for the cold (hot) HeH^+ of $a_2 = 50 \pm 3\%$ ($38 \pm 3\%$) and $a_{-1} = 50 \pm 5\%$ ($62 \pm 1\%$), indeed showing a more even contribution of $^1\Sigma$ and $^1\Pi$ states.

IV. DISCUSSION

A. Comparison to theory

Two recent theory papers specifically addressed the xuv photodissociation of HeH^+ [2,3]. Dumitriu and Saenz [2] made channel-specific calculations of the absolute photodissociation cross section within the Born-Oppenheimer approximation, including 35 states of $^1\Sigma$ and 25 states of $^1\Pi$ symmetry and evaluating explicitly the effect of vibrational excitation of the initial HeH^+. They also discussed several properties of nonadiabatic interactions and calculated energy-resolved cross sections under both complete adiabatic and diabatic assumptions. Sogoda *et al.* [3] performed time-dependent calculations including particularly nonadiabatic couplings associated with the first-derivative operator for the internuclear distance as well as rotational couplings [1] between the $^1\Sigma$ and $^1\Pi$ states for molecular states asymptotically connected with atomic fragments in the $n = 2$–3 excited states of both He and H.

1. Dissociation pathways and nonadiabatic dynamics

It is a clear observation from the present experiment that photodissociation of HeH^+ at 32 nm mainly leads to neutral atomic fragments He($1snl$) or H(nl) of the respective high excitation ($n \gtrsim 3$) in both dissociation channels and is largely independent of the initial vibrational excitation of the molecular ion (see Figs. 6 and 7).

Dumitriu *et al.* [2] predicted that most nonadiabatic couplings (avoided crossings) preserve the channel identity and therefore would be of less importance for evaluating the channel-resolved cross sections; however, they explicitly pointed to the possible importance of nonadiabatic couplings for the distribution of final atomic states. In terms of the absolute cross sections, Sogoda *et al.* [3] found that the pure Born-Oppenheimer calculations did not agree with the experimental result [14], whereas a better agreement was obtained with the inclusion of nonadiabatic interactions. However, as mentioned above, only excitations with $n \leqslant 3$ were considered in the calculation [3], which is inconsistent with the experimental evidence.

Hence, a significant question arising from the present experimental results concerns the origin of the dominant excited Rydberg states for the emerging atomic fragments. On the one hand, their importance may be of a statistical nature (i.e., there are simply more states available for photoabsorption associated with these final limits); on the other hand, their importance could indeed result from nonadiabatic dynamics during the dissociation process, as pointed out theoretically [2,3]. A direct comparison between experiment and theory is not yet possible in terms of final state distributions, since one theory has not calculated these explicitly [2] and the other [3] evidently does not consider the full spectrum of excitations observed experimentally.

2. Channel branching and vibrational excitation

In the experiment we find an asymmetric branching between the two final channels, $He + H^+$ and $He^+ + H$, with a preference for $He^+ + H$ for cold ions, while an almost equal branching is seen for vibrationally hotter ions.

In the relevant range of excitation, the calculation by Dumitriu *et al.* [2] revealed a remarkable energetic separation of the adiabatic potential curves leading to the He($1snl$) + H^+ channel and those leading to the $He^+ + H(nl)$ channel. Most of the lower-lying states correlate to $He + H^+$ while the highest Rydberg states correlate to $He^+ + H$. In calculations on rovibrationally cold ions, the relative importance of the two channels was found [2] to depend strongly on the photon energy, with the $He^+ + H$ channel being dominant until ~35 eV, above which the two channels were predicted to be of about equal importance. In particular at 38.7 eV (32 nm), the cross sections (as inferred from Figs. 5 and 6 of Ref. [2]) are $\sigma_{He^+ + H} \sim 2.5$ Mb and $\sigma_{He + H^+} \sim 1.5$ Mb, resulting in a branching ratio of ~1.6. This agrees very well with our experimental result of 1.70 ± 0.48 for vibrationally cold ions.

The experimental finding that this branching ratio gets smaller (0.96 ± 0.11), that is, more dissociation proceeds to the $He + H^+$ channel, with higher vibrational excitation, seems contradictory to the above-mentioned separation of the potential curves leading to the two dissociation channels [2]. Thus, with higher vibrational excitation of the initial HeH^+, the Franck-Condon region accessible in photoabsorption extends to higher values of the internuclear distance, whereby more states leading to $He^+ + H$ would become available for photoabsorption. Hence, the experimental results cannot easily be rationalized, considering the general nature of the theoretically predicted adiabatic potential landscape in the region 38–39 eV [2]. This observation could indeed be another indication of the significance of nonadiabatic interactions in the dissociation process. It should be noted, however, that direct ionization into the $He^+(1s) + H^+$ continuum could also become possible for vibrational excited states at 32 nm [4]; such events would appear as H^+ in the present experimental determination of the channel branching ratio.

Sodoga *et al.* [3] particularly pointed out the importance of nonadiabatic couplings for the branching of the two dissociation channels in the region of 35 eV photon energy, where a prominent avoided crossing occurs. This would indeed be an interesting aspect to investigate in future experiments.

3. The photoabsorption process

Experimentally we have access to information on the photodissociation process through an estimate of the absolute dissociation cross section, as shown in our previous experiment [14], and with better sensitivity through the angular distributions [Figs. 6(c) and 7(b)] of fragments relative to the laser polarization. The uncertainty associated with the absolute cross section is mostly determined by systematic errors and to a lesser extent by the statistical error. Therefore, the present measurements do not offer more information on this aspect than what was given previously [14]. On the other hand, assuming a prompt dissociation process, the fragment angular distributions hold direct information on the symmetry of the absorbing state ($^1\Sigma$ or $^1\Pi$).

Interestingly, here we observe different fragment asymmetries for the two final dissociation channels. For $He + H^+$, we find a dominance of absorption through Π states (i.e., $^1\Sigma$:$^1\Pi \sim 3$:7, consistent with our previous measurement, while for the $He^+ + H$ channel, we observe $^1\Sigma$:$^1\Pi \sim 4$:6 for

hot ions and ∼1:1 for cold ions. Around the experimental energy of 38.7 eV, the calculation of Dumitriu *et al.* [2] shows good agreement with the experimental results for the $He + H^+$ channel, predicting a similar angular ratio $^1\Sigma:^1\Pi \sim 1:2$ (from Fig. 6 of Ref. [2]). However, for the $He^+ + H$ channel, the calculation predicts $^1\Sigma:^1\Pi \sim 1:6$ (extracted from Figs. 5 and 6 of Ref. [2]), in strong contrast to the observed ∼1:1 experimental result for cold ions.

B. Development of experimental methods

In the previous experiment [14], establishing the feasibility of experiments on fast ion-photon interaction at a free-electron laser (FEL), we studied the photofragmentation of vibrationally hot HeH^+ fragmenting into the $He + H^+$channel. In the present measurements, we have significantly expanded the study by characterizing also the second dissociation channel ($He^+ + H$) and performing measurements for both vibrationally cold and hot ions. The development of a new detector [15] was essential for access to the light fragments (H and H^+). Moreover, in the present study, vibrational cooling of the molecular ions in the electrostatic ion trap prior to irradiation by FLASH could also be applied.

The strength of the photodissociation signal was considerably increased in comparison to the previous experiment, both through a higher and more stable photon flux from FLASH and through higher ion-beam intensity. The signal-to-background ratio was increased due to the improved quality of photon flux.

In the earlier experiment [14], a high negative potential was applied at the interaction region to effectively suppress background by a large shift of the time of flight of the neutral photofragment fragment (He). In the present experiment we used a smaller positive potential to actively separate charged and neutral fragments. For the $He + H^+$ channel, we could further essentially eliminate background by the use of coincidence detection.

V. CONCLUSION

In this paper, we have addressed the dissociation dynamics of HeH^+ through the manifold of excited states that arises from the excitation of a valence electron. The experiment takes explicit advantage of the unprecedented intensities and timing structure of xuv pulses available at the FLASH facility [12,13] to perform kinematically complete characterizations of individual dissociating HeH^+ ions after cooling the ions to the vibrational ground state in an electrostatic ion trap.

For atomic fragments of different types, $He(1snl)$ and $H(nl)$, photodissociation of HeH^+ at 32 nm was shown to proceed mainly toward highly excited states, $n \gtrsim 3$–4. The trend in the photodissociation dynamics revealed by this observation appears to be conserved over the different regions of internuclear distances probed using vibrationally hot and cold HeH^+. The origin of this dissociation dynamics remains an open question, whose solution would likely have to consider nonadiabatic couplings. For vibrationally cold ions, the two product channels $He(1snl) + H^+$ and $He^+(1s) + H(nl)$ were found at a ratio of $\sigma_{He^+ + H}/\sigma_{He+H^+} = 1.70 \pm 0.48$, in excellent agreement with a recent theoretical prediction [2], while they become of about equal significance for vibrationally hotter ions.

The photoabsorption process was determined to be dominated by $^1\Pi$ states for the $He(1snl) + H^+$ channel ($^1\Sigma:^1\Pi \sim 3:7$) while more even contributions were seen for the $He^+(1s) + H(nl)$ channel ($^1\Sigma:^1\Pi \sim 1:1$, cold ions). The latter finding is not expected in the present theoretical descriptions [2] and represents another interesting aspect of future investigations.

In a perspective, upcoming measurements could focus on both the region of lower photon energy, where explicit effects of nonadiabatic interactions are predicted [2,3], as well as on higher energies, where inner and outer valence ionization additionally become possible [4].

ACKNOWLEDGMENTS

This work has been supported by the Minerva Foundation, the Max-Planck Initiative DESY FEL (MIDFEL), and the Max-Planck Advanced Study Group. HBP acknowledges support from the Lundbeck foundation. We are greatly indebted to the scientific [12,13] and technical team at FLASH.

[1] H. Lefebvre-Brion and R. W. Field, *Pertubations in the spectra of Diatomic Molecules* (Academic, New York, 1986).
[2] I. Dumitriu and A. Saenz, J. Phys. B **42**, 165101 (2009).
[3] K. Sodoga, J. Loreau, D. Lauvergnat, Y. Justum, N. Vaeck, and M. Desouter-Lecomte, Phys. Rev. A **80**, 033417 (2009).
[4] J. Fernandez and F. Martin, J. Phys. B **40**, 2471 (2007).
[5] D. Galli and F. Palla, Astron. Astrophys. **335**, 403 (1998).
[6] I. Dabrowski and G. Herzberg, Ann. NY Acad. Sci. **38**, 14 (1977).
[7] S. Jonsell, A. Saenz, and P. Froelich, Phys. Rev. C **60**, 034601 (1999).
[8] N. Doss and J. Tennyson, J. Phys. B **41**, 125701 (2008).
[9] C. Weinheimer, Prog. Part. Nucl. Phys. **57**, 22 (2006).
[10] M. Kling *et al.*, Science **312**, 246 (2006).
[11] M. Kremer *et al.*, Phys. Rev. Lett. **103**, 213003 (2009).
[12] W. Ackermann *et al.*, Nat. Photonics **1**, 336 (2007).
[13] K. Tiedtke *et al.*, New J. Phys. **11**, 023029 (2009).
[14] H. B. Pedersen *et al.*, Phys. Rev. Lett. **98**, 223202 (2007).
[15] H. B. Pedersen *et al.*, Phys. Rev. A **80**, 012707 (2009).
[16] M. Martins, M. Wellhöfer, J. T. Hoeft, W. Wurth, J. Feldhaus, and R. Follath, Rev. Sci. Instrum. **77**, 115108 (2006).
[17] T. S. Green, Rep. Prog. Phys. **37**, 1257 (1974).
[18] D. Zajfman, O. Heber, L. Vejby-Christensen, I. Ben Itzhak, M. Rappaport, R. Fishman, and M. Dahan, Phys. Rev. A **55**, R1577 (1997).
[19] Z. Amitay, D. Zajfman, and P. Forck, Phys. Rev. A **50**, 2304 (1994).
[20] H. B. Pedersen *et al.*, Phys. Rev. A **72**, 012712 (2005).
[21] J. Purder, S. Civis, C. E. Blom, and M. C. van Hemert, J. Mol. Spectrosc. **153**, 701 (1992).
[22] Z. Liu and P. B. Davis, J. Chem. Phys. **107**, 337 (1997).
[23] R. N. Zare, Mol. Photochem. **4**, 1 (1972).